JOURNAL OF GEOPHYSICAL RESEARCH, VOL. 86, NO. B8, PAGES 7027–7036, AUGUST 10, 1981

The Bermuda Earthquake of March 24, 1978: A Significant Oceanic Intraplate Event

GORDON S. STEWART AND DONALD V. HELMBERGER

Seismological Laboratory, California Institute of Technology, Pasadena, California 91125

The Bermuda earthquake ($M \sim 6$) occurred near the westerly extension of the Kane Fracture Zone roughly 370 km southwest of the island of Bermuda. It is one of the largest oceanic intraplate earthquakes to occur off the eastern coast of North America. Because of its size and location, it has provided an excellent set of WWSSN body waves. They can be used to infer its depth and faulting parameters by waveform modeling techniques. The results indicate a north-northwest striking thrust mechanism (strike = N20°W, dip = 42°NE, rake = 90°) with the hypocenter located at a depth of 11 km, which for an oceanic crust places it predominantly in the mantle. The event had a seismic moment of 3.4×10^{25} dyne cm, and its time history was modeled with a symmetric trapezoidal time function 3 s in duration. The north-northwest strike of the event is in good agreement with the bathymetry of the area, the epicenter being close to the southwestern edge of the Bermuda Rise. The strike of the event is also close to that of the inferred extensions of the present ridge fracture zones in the region. The presence of such fracture zones is indicative of local weak zones in the lithosphere. The Bermuda earthquake most likely is associated with one of these zones of weakness and is the result of the application of present day stress imposed on the region by the North American plate in the direction of its absolute motion. This is an important event in terms of understanding and estimating seismic hazard on the eastern seaboard of North America.

INTRODUCTION

The Bermuda earthquake of March 24, 1978 (origin time: 0042:37.7 UT; location: 29.9°N, 67.3°W; depth: 11 km (this study); $m_b = 6.1$, $M_s = 5.8$) is one of the largest eastern North American plate events to occur since the installation of the World-Wide Standardized Seismographic Network (WWSSN) in 1963. Because of the size and location of this event (Figure 1) it was well-recorded by the WWSSN, and in particular it provided a high-quality body wave data set suitable not only for the analysis of the source properties of the event itself but also for the study of the upper mantle structure beneath eastern North America [*Stewart and Helmberger*, 1979; J. W. Given et al., manuscript in preparation, 1981]. This paper deals with a detailed analysis of the body waves from the event and the constraint that this data places on the various source parameters of the Bermuda earthquake. The event is located within the oceanic plate off the coast of eastern North America, 370 km southwest of Bermuda. As such, it is the largest event to have occurred there since seismographic recording began. It was widely felt along the southeast coast of the United States. Because of the paucity of well-recorded earthquakes from the area, it is an important event to study since it may help elucidate the tectonic origin of intraplate events, especially within the environment of eastern North America.

Results from the analysis of *P* wave and *SH* wave first motions and waveforms in this study indicate that the event had a pure thrust mechanism with planes of approximately 45° dip, striking in a north-northwest direction. It was located at a depth of 11 km, predominantly below the Mohorovicic discontinuity, a somewhat unusual result which was required by the high-quality data set. The earthquake occurred close to zones of weakness of ancient fracture zones in the proximity of a major zone of plate motion disruption at magnetic anomaly M11 (~125 m.y. B.P.), the time when the south Atlantic began opening. This resulted in local changes in spreading direction and plate velocity in this region. The Bermuda earthquake occurred as a result of the application of present-day stress imposed on the region by the North American plate in the direction of its absolute motion.

Paper number 1B0745.
0148-0227/81/001B-0745$01.00

BODY WAVE ANALYSIS

In order to constrain the source parameters such as focal mechanism, size, depth, and time function for the Bermuda earthquake, a complete study of the body waves from the event was made. The data, which were taken primarily from WWSSN and Canadian long-period seismograms, consist of *P* wave first motions, *SH* polarities, and *P* and *S* waveforms. *P* wave first-motion data, which were read in this study, are plotted in Figures 2*a* and 2*b*. Initially, a hypocenter which was located in the crust with a source velocity of 6.3 km/s, as shown in Figure 3 (star) was assumed. This resulted in the focal mechanism plot shown in Figure 2*a*. The long-dashed planes show a solution similar to that published by *Nishenko et al.* [1978]. The short-dashed fault planes show another possible solution. However, both mechanisms are inconsistent with several good quality first-motion data, and no solution is possible without contradiction of at least some of these data points. If instead, the hypocenter is located in the mantle, where the source velocity is 8.0 km/s, as shown in Figure 3 (asterisk), the station positions are shifted outward on the focal sphere and the result is given in Figure 2*b*. Now it is possible to draw fault planes that can separate well the compressional and dilatational fields. In particular, stations LPS, SJG, and BEC, some or all of which previously were inconsistent, now plot in the appropriate dilatational areas. To verify this solution, obtain a depth and time function for the event, and study the degree of complexity of the source, synthetic seismograms were calculated and compared with the observed data. Neither of the *P* wave solutions shown in Figure 2*a*, with the source located in the crust, could explain the *P* and *SH* waveforms shown in Figures 4 and 7.

P WAVE ANALYSIS

An initial look at the observed *P* wave seismograms, shown in Figure 4, indicates a complex sequence of arrivals at most stations. It was not known at first what this complexity was

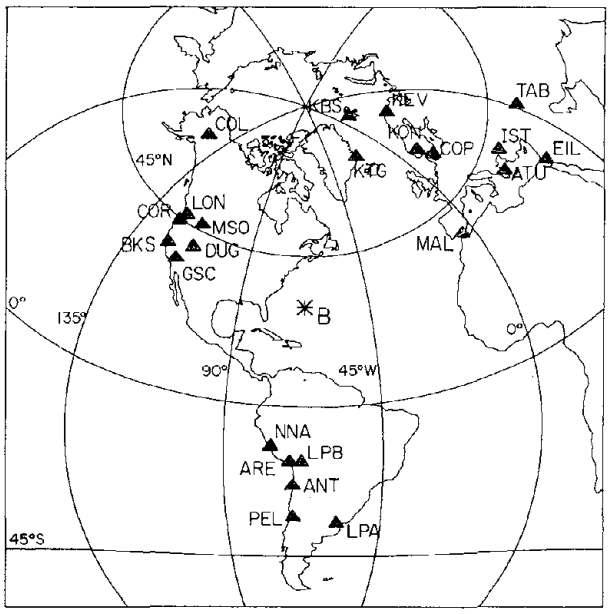

Fig. 1. Map showing locations of 23 WWSSN stations used in the *P* wave modeling of the Bermuda earthquake. Note the good azimuthal coverage of stations around the epicenter (B). An azimuthal equidistant projection is shown. See Table 1 for distances and azimuths.

due to. At the beginning of the trace the pulse looks relatively simple and of larger amplitude than the later arrivals. Since the source is located beneath the ocean, the later arrivals could be due to water reverberations, which have been observed previously on vertical long-period seismograms for sources below a water layer [*Ward*, 1979]. Another possibility is that the complicated waveforms might be due to complexity in the source dislocation process itself, for example, as from *Butler et al.* [1978], *Kanamori and Stewart* [1978], *Rial* [1978], and *Stewart and Kanamori* [1978]. To examine this question further, synthetic *P* wave seismograms were calculated for a point source beneath a layered crust, and the results compared with the observed data. If satisfactory fits could be found using a single point source, then the source could be regarded as simple, and the complexity of the waveforms would be due to interactions with the source crustal structure rather than to the source itself.

A particular advantage in this study is the epicentral location of the Bermuda earthquake. As shown in Figure 1 and in Table 1, the event is centered in an area that provides an excellent azimuthal coverage of WWSSN stations in appropriate distance ranges for the study of *P* waveforms, i.e., 30° to 90°. The observed *P* waveforms from vertical long-period instruments are shown in Figure 4 along with the station positions on the focal sphere. At first glance, data in different azimuths look similar, i.e., one large initial pulse followed by later arrivals. However, on closer examination some differences exist. For example, stations KBS, TAB, EIL, LPB, ANT, and COL have large initial upswings compared with the second upswings. For stations such as KON, COP, NNA, BKS, and MSO the second upswing is comparable to or slightly greater than the amplitude of the first upswing, while for stations MAL and GSC the initial upswing is low in amplitude compared with the second and might be regarded as almost nodal in character. Although these variations are subtle for some stations, there do appear to be overall differences in the initial *P* wave shape. An attempt to match these was made by generating synthetic waveforms. No crustal structure information was obtainable for the epicentral region of the Bermuda event. However, in the vicinity of Bermuda itself and to the northwest and southeast of the island, several refraction studies have been made. They are presented by *Officer et al.* [1952] and *Ewing et al.* [1954], and the resulting crustal structure is shown in Figure 3 in a modified form. This structure was considered to be appropriate for the crust beneath the Bermuda epicenter. We chose to omit a 1.2-km-thick sedimentary layer of velocity 2 km/s from the top of the crust since such a layer made only negligible differences to the synthetic waveforms and would not be resolvable in the ob-

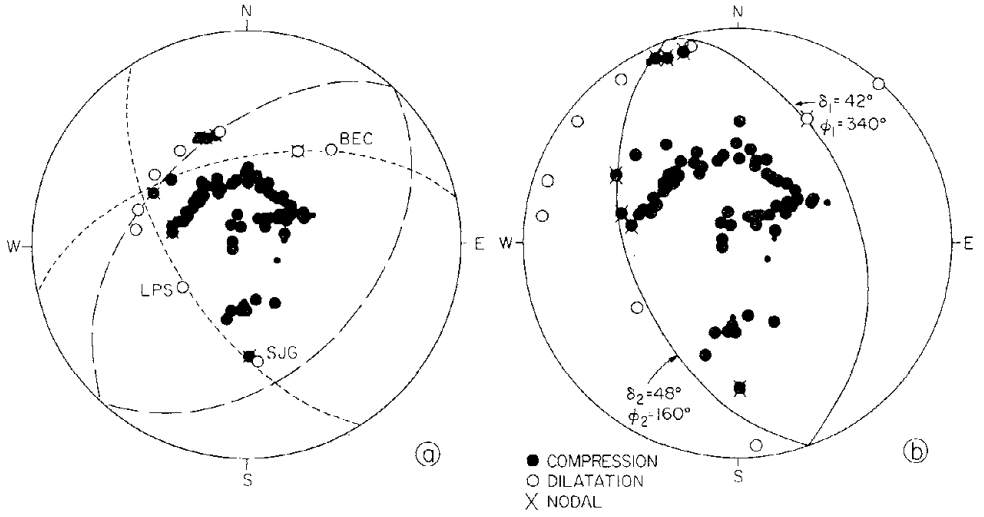

Fig. 2. (*a*) The *P* wave first-motion data for the Bermuda earthquake of March 24, 1978, with the hypocenter located in the crust (see Figure 3 (star)). Note that the first-motion data plot closer to the center of the focal sphere compared with the data for a source in the mantle (Figure 2*b*). In this case, two orthogonal focal planes cannot be fit to the data without violating several very good *P* wave readings. The pure thrust mechanism shown (long-dashed planes) is similar to that obtained by *Nishenko et al.* [1978]. Another possible solution is indicated by the short-dashed planes. (*b*) The *P* wave first-motion data for the Bermuda earthquake of March 24, 1978, with the hypocenter located in the mantle (see Figure 3 (asterisk)). The mechanism indicates approximately 45° pure thrust faulting on a plane striking N20°W. The actual fault plane and auxiliary plane cannot be distinguished. Data used in this plot were read mainly from WWSSN seismograms in this study. An equal area projection of the lower focal hemisphere is shown in both Figures 2*a* and 2*b*.

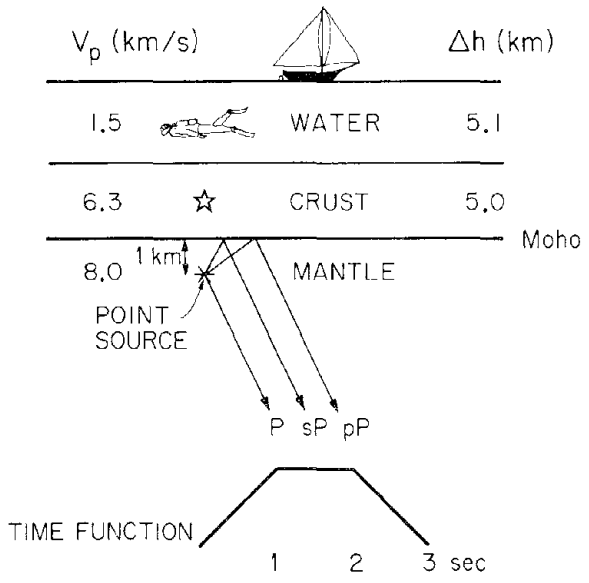

Fig. 3. Velocity structure used in this study (modified from *Officer et al.* [1952] and *Ewing et al.* [1954]). The star indicates a crustal hypocenter, while the asterisk indicates a hypocenter located 1 km beneath the Mohorovicic discontinuity, the preferred location. The time function used in the modeling of the source is also shown.

served data. Omitting this layer also simplifies the presentation. Using the crustal structure shown in Figure 3 and a point source in the mantle, *P* wave synthetic seismograms were generated using the method described by *Langston and Helmberger* [1975] and *Langston* [1976]. Rays *P*, *pP*, and *sP* are shown in Figure 3 leaving the source region. Here, *pP* and *sP* are reflections from the base of the crust. However, to explain the initial pulse on the *P* wave seismograms, additional rays have to be included. They result from the energy transmitted into the crust and water layers by upgoing *P* and *S* wave radiation, the source conversions of *P* to *S* and *S* to *P* at the various interfaces and eventually transmitted to the mantle, and multiple reflections of *P*, *S*, and combinations of these within and between the crust and water layers. In all, for an adequate modeling of the initial pulses shown in Figure 4, 22 rays were used. Their description is given in Figure 5*a*. As a check and for the final modeling shown in Figure 4, the modification of the Thomsen-Haskell layered matrix method by *Harkrider* [1964], *Douglas et al.* [1974], and *Langston* [1976] was employed. This allowed us to model easily the *P* wave train for the first 1.5 min of record. The later energy comes from *P* wave reflections within the water layer, and because of the high reflection coefficient at the water-crust interface, the amplitude decay of this reverberation is slow. From an amplitude comparison of observed with synthetic *P* waveforms an averaged seismic moment of $M_o = 3.4 \times 10^{25}$ dyne cm was obtained. Individual values for some of the stations are given in Table 1. The depth and time functions were varied in the above *P* wave analysis and in the later *SH* wave analysis. The best fits obtained, consistent with both *P* and *S* wave data are for a point source located 1 km beneath the Mohorovicic discontinuity, with a 3-s duration time function, as shown in Figure 3. In the *P* wave modeling a t^* value of 1.0 was used.

S Wave Analysis

Many of the WWSSN stations were favorably located with respect to *P* wave radiation from the Bermuda source, as discussed in the previous section on the *P* wave analysis. The same fortunate circumstance applied to the distribution of WWSSN and Canadian stations for the *S* waves. The stations

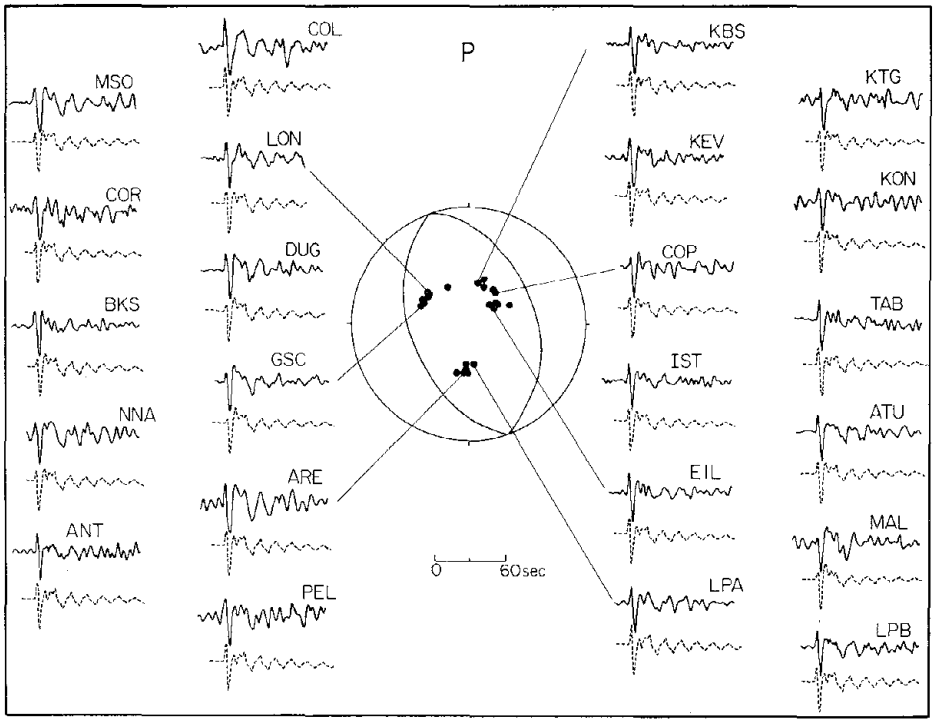

Fig. 4. Observed (upper) and synthetic (lower) *P* wave traces from the vertical long-period WWSSN seismograms for stations shown in Figure 1 and listed in Table 1. Note an initial simple event followed by more complicated water reverberations. The fault plane solution from Figure 2*b* is shown in the center, along with the locations of the *P* wave stations on the focal sphere (solid circles).

TABLE 1. Station Parameters

Station	Δ, deg	ϕ_{ES}	ϕ_{SE}	C or D	$M_0 \times 10^{25}$ dyne cm	Waves Used‡
			WWSSN			
AAE	99.21	74.1	302.3	C		*P*
AAM	18.07	317.6	127.9	C		*P*
ALQ	33.29	289.0	87.5	C		*P*
ANT	53.37	183.6	3.4	C	2.55	*P, PW, S, SW*
AQU	64.11	54.4	287.7	C		*P*
ARE	46.26	185.6	5.0	C		*P, PW, S, SW*
ATL	14.93	288.0	99.0	D		*P*
ATU	73.05	55.7	294.8	C		*P, PW*
BDF	49.00	154.9	337.5	C		*P*
BEC	3.34	41.6	222.9	D		*P*
BKS	45.74	295.2	83.0	C	5.79	*P, PW, S, SW*
BLA	13.14	307.1	119.9	D		*P*
BOG	25.94	195.6	13.5	C		*P*
CAR	19.30	178.9	359.0	C*		*P*
COL	59.35	330.7	84.5	C	2.45	*P, PW, S*
COP	60.24	39.9	280.2	C	4.54	*P, PW, S*
COR	46.06	304.6	88.8	C	3.44	*P, PW, S, SW*
CTA	148.16	280.0	65.5	C		*PKP*
DAG	52.05	12.6	235.6	C		*P, S, SW*
DAL	25.31	284.3	88.7	C*		*P*
DAV	141.20	339.3	18.0	C		*PKP*
DUG	38.29	298.1	91.0	C		*P, PW*
EIL	85.25	58.7	301.6	C		*P, PW*
EPT	33.59	283.3	82.7	C		*P*
ESK	51.41	41.1	268.0			*S*
FVM	20.78	299.0	106.0	C		*P*
GDH	40.19	7.6	198.7	C		*P, S*
GRM	108.67	118.1	293.9	C†		*PKP*
GSC	41.71	290.8	83.0	C	4.15	*P, PW*
GUA	126.82	319.6	35.3	C		*PKP*
IST	75.38	51.0	296.9	C	3.99	*P, PW, S*
JCT	28.05	279.4	82.8	C*		*P*
KBS	58.81	12.8	265.8	C	3.74	*P, PW, S, SW*
KEV	63.76	22.8	285.1	C	2.90	*P, PW, S*
KJF	65.63	28.6	288.3	C		*P*
KOD	127.64	45.8	320.8	C		*P*
KON	58.20	35.6	275.6	C	3.56	*P, PW, S, SW*
KTG	47.72	18.9	236.6	C	2.77	*P, PW, S*
LON	45.03	307.7	92.0	C		*P, PW*
LPA	65.06	171.5	351.0	C	4.25	*P, PW, S, SW*
LPB	46.16	181.1	1.0	C	4.01	*P, PW, S, SW*
LPS	25.45	237.1	48.8	D		*P*
LUB	29.55	286.1	87.6	C		*P*
MAL	52.18	64.9	281.9	C	2.98	*P, PW, S*
MSO	39.65	308.5	98.4	C	2.77	*P, PW, S*
NAI	102.85	84.0	300.2	C†		*PKP*
NDI	112.61	33.6	326.9	C†		*PKP*
NNA	42.64	193.9	12.3	C	2.04	*P, PW, S, SW*
NUR	65.40	33.0	287.3	C		*P*
OGD	12.63	333.9	149.6	C*		*P*
PDA	35.24	65.9	269.8	C†		*P*
PEL	62.77	183.2	3.3	C†	2.97	*P, PW*
PTO	48.26	59.9	276.1	C		*P*
QUE	106.06	40.2	319.7	C		*PKP*
RIV	147.23	253.0	86.2	C		*PKP*
SCP	13.87	324.5	138.4	D		*P*
SHA	18.02	277.7	87.2	D		*P*
SHI	97.58	49.7	310.5	C		*P*
SHK	113.21	342.1	18.8	C		*PKP*
SHL	121.35	22.1	338.8	C		*P*
SJG	11.78	174.6	355.1	D		*P*
STU	59.66	48.2	281.8	C		*P, S*
TAB	88.30	46.3	307.3	C	2.98	*P, PW, S*
TOL	51.87	60.9	279.7	C		*P*
TUC	37.12	285.1	81.9	C		*P*
WES	12.87	346.5	164.1	D		*P*
Average					3.4	
			Canadian			
ALE	52.74	0.8	85.3	C		*P*
EDM	40.65	318.3	106.3	C		*P*
FCC	34.18	335.3	135.9	C		*P*

TABLE 1. (continued)

Station	Δ, deg	ϕ_{ES}	ϕ_{ES}	C or D	M_0, × 10^{25} dyne cm	Waves Used‡
			Canadian (continued)			
FFC	35.09	325.0	120.7	C		*P*, *S*
FRB	33.87	359.0	178.1	C		*P*
FSJ	47.22	318.1	97.4	C		*P*
LHC	24.98	323.8	129.7	C		*P*
INK	53.08	328.9	96.4	C		*P*
MBC	52.46	346.2	120.3	C*		*P*
MNT	16.34	344.1	160.2	C*		*P*
OTT	16.82	339.1	154.0	C*		*P*
PHC	48.88	312.9	91.4	C		*P*
PNT	43.74	311.5	96.4	C		*P*
RES	46.95	350.3	146.6	C		*P*
SCH	24.91	0.7	181.1	C		*P*
SES	34.48	314.7	105.4	C		*P*
STJ	20.92	28.5	217.7	D*		*P*
VIC	46.18	310.1	92.5	C		*P*
YKC	44.50	330.9	114.6	C		*P*
			IDA			
CAN	149.19	250.9				*R*1, *R*2
CMO	59.32	330.7				*R*1
GAR	100.80	32.2				*R*1
NNA	42.64	193.9				*R*1, *R*2
PFO	41.66	288.3				*R*2, *R*3
RAR	102.40	252.8				*R*1
SUR	103.97	119.2				*R*1, *R*2

The ϕ_{ES} is the azimuth of the station from the epicenter; ϕ_{SE} is the azimuth of the epicenter from the station.

* Nodal reading.

† Poor reading.

‡ *P*, *P* wave first motion used; *PKP*, *PKP* wave first-motion used; *S*, *S* wave polarity used; *PW*, *P* waveform used; *SW*, *S* waveform used; and *R*1, *R*2, and *R*3, multiple Rayleigh wave used.

grouped in three dominant areas of the world, i.e., North America, South America, and Europe. This can be seen in Figure 6 and in Table 1 and is shown by the solid circles in Figure 7. Also from Figure 6 and Table 1 it can be noted that most of these stations are close to being naturally rotated into pure *SH* and *SV* radiation with respect to the *S* waves from the Bermuda event. For stations in North America and Europe, *SH* waves are well-recorded on the north-south components, *SV* waves on the east-west components, while in South America *SH* waves record well on the east-west components, *SV* on the north-south components. This fortunate occurrence allowed easy identification of the waveforms and polarities of *SH* and *SV* waves to be made. These polarities were read from as many of the WWSSN and Canadian stations as possible. All *SV* waves showed negative polarity or motion toward the source. The *SH* wave polarities are plotted in Figure 7. Here positive polarity corresponds to clockwise motion. Representative *S* wave seismograms from different azimuths from the earthquake source were rotated, as necessary, and the resulting *SH* waves plotted in Figure 7. The solid lines on the focal sphere represent nodes in the *SH* wave radiation which are consistent with the *P* wave focal mechanism shown in Figure 2*b*. Note that the polarity of the observed records changes with azimuth in moving from one quadrant to the next. Again, as for the *P* waves, there are differences in the waveforms. The *SH* waveforms for stations DAG and KBS show almost symmetric waveforms as far as the first (positive) and second (negative) pulses are concerned. On the other hand, the data from stations LPA, LPB, ARE, and BKS show an asymmetric waveform having a narrower first pulse and broader second pulse. Presumably, these features should be reproduced synthetically if we can find the proper choice of source parameters. With a point source located in the mantle, as shown in Figure 3, synthetic *SH* waveforms were generated and matched to the data. In this case, only five rays proved to be significant, and they are sketched in Figure 5*b*. At first, the mechanism shown in Figure 2*b* was

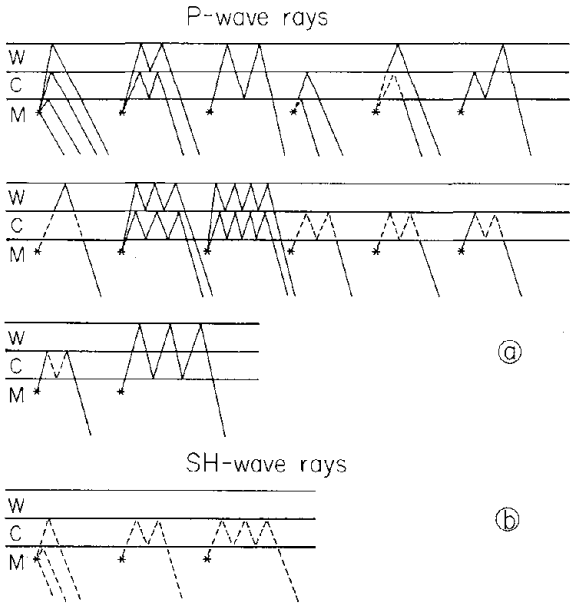

Fig. 5. (*a*) Schematic figure showing the 22 rays used in the modeling of the *P* wave synthetics for the Bermuda earthquake. Solid lines represent *P* waves; dashed lines represent *SV* waves. Note that the rays shown include direct reflections, *P* to *S* and *S* to *P* conversions, and multiple reflections at the various boundaries. (W, water; C, crust; M, mantle). (*b*) Schematic figure showing the five rays used in the modeling of the *SH* wave synthetics for the Bermuda earthquake. Dashed lines represent *SH* waves.

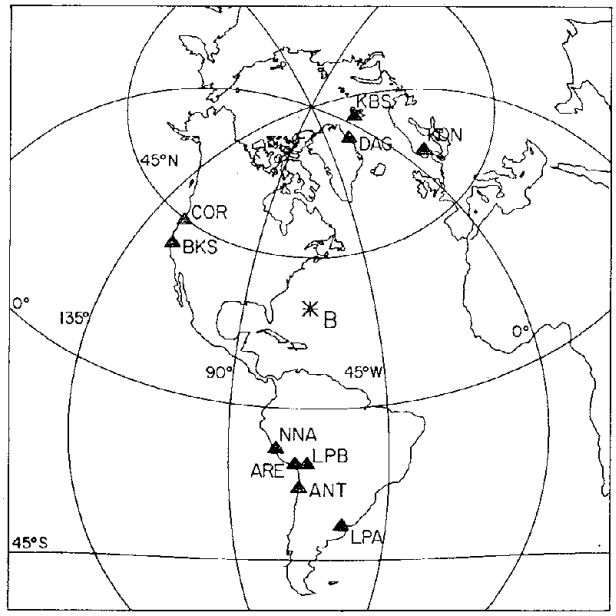

Fig. 6. Map showing locations of 10 WWSSN stations used in the *S* wave modeling of the Bermuda earthquake. Note the good azimuthal coverage of stations around the epicenter (B). An azimuthal equidistant projection is shown. See Table 1 for distances and azimuths.

tried, with a dip of 45° ascribed to both planes. The depth and time functions were varied as in the *P* wave analysis with a t^* value of 4.0 being used for the *S* wave modeling. The best result produced waveforms with polarities which agreed with the observed data. However, both the first and second pulses were symmetric, and the narrow first pulse, broad second pulse feature was not observed. This effect could be explained by changing the dips of the northeast and southwest dipping planes to 42° and 48°, respectively, as shown in Figure 2*b*. The *SH* wave synthetics for this model are shown in Figure 7. For stations to the southwest of nodal line AB of Figure 7, direct *S* becomes less nodal and *sS* more nodal than for the 45° case. Stations to the northeast of line AB have the opposite effect, with a less dramatic effect on the resulting waveforms. The nodal line CD remains the same with the change in dip angle of the fault planes away from 45°. Thus, modeling of a set of *SH* polarities and waveforms for the Bermuda earthquake gives results consistent with those obtained from *P* wave first motions and *P* waveform modeling. The source mechanism indicated in Figure 2*b* and velocity model shown in Figure 3 with the hypocenter 1 km below the Mohorovicic discontinuity are preferred over that with either of the mechanisms indicated in Figure 2*a* and a crustal source. *SV* polarities and waveforms obtained from the WWSSN and Canadian stations are all identical and so provide no additional constraint other than being consistent with this mechanism.

The *P* wave coda discussed earlier could be explained successfully by simply adding in the contributions of the many rays partially trapped in the water layer. However, the *SH* wave coda appears much more complicated and difficult to explain. Complicated *S* wave trains have been observed for other non strike slip events [see *Langston*, 1978; *Langston and Butler*, 1976]. On the other hand, the *SH* wave trains observed for pure strike slip events at the appropriate *SH* loop maxima are remarkably simple, as in the work by *Helmberger and Engen* [1974]. These observations suggest that the above complications occur in the presence of strong *SV* motions in the source region at ray parameters not far removed from those appropriate for *SH* and may, in fact, be *SV*-to-*SH* conversions caused by nonplanar structure; see, for instance, *Langston* [1978].

Surface Wave Analysis

As a check on the focal mechanism solution from our body wave analysis and in order to estimate a long-period surface wave moment, the Rayleigh waves excited by the Bermuda earthquake were analyzed. The records we used in the analysis were produced by the International Deployment of Accelerographs (IDA) worldwide network of digitally recording gravimeters discussed by *Agnew et al.* [1976]. The data used consisted of *R*1, Rayleigh waves from six IDA stations (CAN, Canberra, Australia; CMO, College, Alaska; GAR, Garm, USSR; NNA, Nana, Peru; RAR, Raratonga, Cook Islands; and SUR, Sutherland, South Africa), *R*2 waves from four stations (CAN, NNA, PFO (Pinon Flats, California), and SUR), and *R*3 waves from PFO. The method of analysis, described by *Kanamori and Given* [1981], uses these wave amplitudes at a period of 165 s. The amplitudes are corrected for distance assuming the spherically symmetric earth model and attenuation described by *Kanamori and Given* [1981]. The resulting station relative amplitudes are plotted in Figure 8 as a function of azimuth around the source. Synthetic radiation patterns were then determined for each of the focal mechanisms shown in Figures 2*a* and 2*b* and are also plotted in Figure 8.

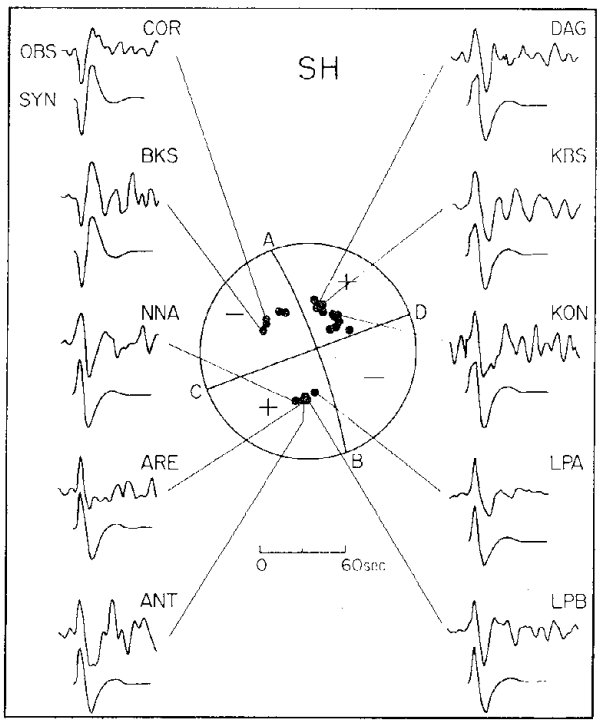

Fig. 7. Observed and synthetic *SH* wave traces, computer rotated from the horizontal long-period WWSSN seismograms for the stations shown in Figure 6. The *SH* wave focal mechanism solution is shown in the center along with the locations of the *S* wave stations on the focal sphere (solid circles). The stations shown in the figure are plotted along with stations for which the polarities of *SH* waves were determined. The positive and negative quadrants represent clockwise and counterclockwise directions of first motion, respectively, for *SH* waves.

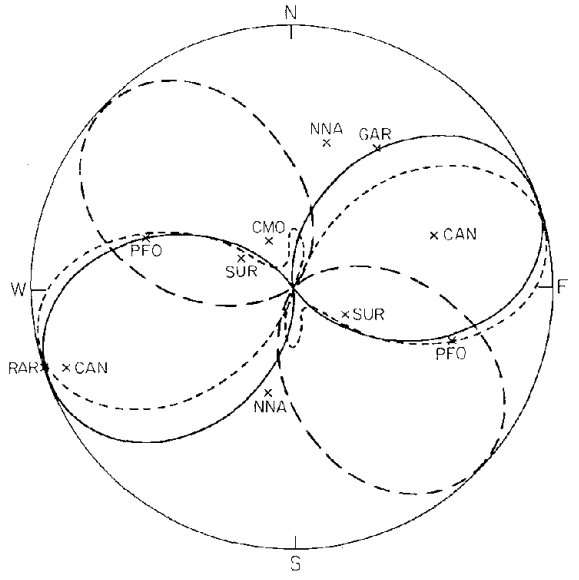

Fig. 8. Amplitudes as a function of azimuth for $R1$, $R2$, and $R3$ surface waves at 165-s period for IDA stations (crosses) which recorded the Bermuda event. The solid curve represents the synthetic radiation pattern for the preferred mechanism (Figure 2*b*). The dashed curves are for the solutions shown in Figure 2*a* and do not fit the data as well.

The dashed curves, which are the radiation patterns for the mechanisms in Figure 2*a*, do not fit the observed data as well as the solid curve which is the pattern for the preferred mechanism for the Bermuda earthquake (Figure 2*b*). By matching the observed data to the synthetic calculations, a long-period surface wave moment of 3.1×10^{25} dyne cm was obtained. This is in good agreement with the value of 3.4×10^{25} dyne cm determined from the P wave data.

Discussion

The island of Bermuda is a topographic peak on the elevated Bermuda Rise or Pedestal and is shown in bathymetric maps by *Chase* [1975] and *Shuran* [1971]. The 1978 event occurred off the southwest point of the Bermuda Rise at its junction with the Hatteras Abyssal Plain, near the 5000-m bathymetric contour. It is interesting to note that the strike obtained for the Bermuda event mechanism is in reasonable agreement with the strike of the steep slope between the Bermuda Rise and the Hatteras Abyssal Plain, namely, north-northwest. The extent of rupture from 11 km toward the surface is unknown. However, the body wave modeling implies that it is not significant.

The oceanic crust in this region is relatively old, the epicenter occurring in Mesozoic crust of Lower Cretaceous age, approximately 125 m.y. old [*Heezen and Fornari*, 1975]. From

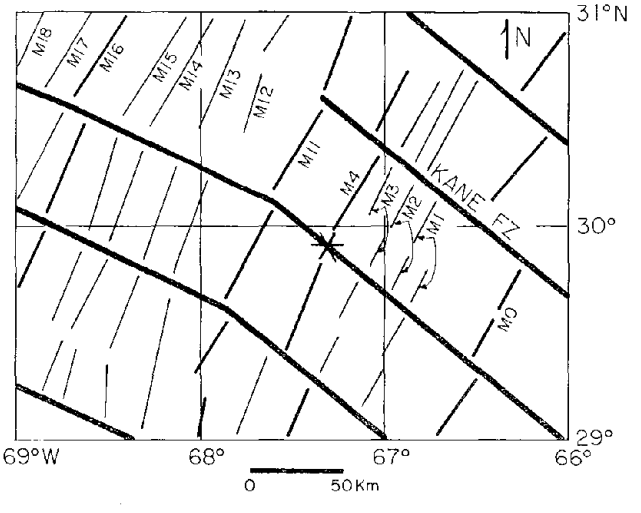

Fig. 9. Map, modified from *Schouten and Klitgord* [1980] indicating the locations of magnetic anomalies and inferred fracture zones in the western Atlantic in the vicinity of the Bermuda earthquake (asterisk).

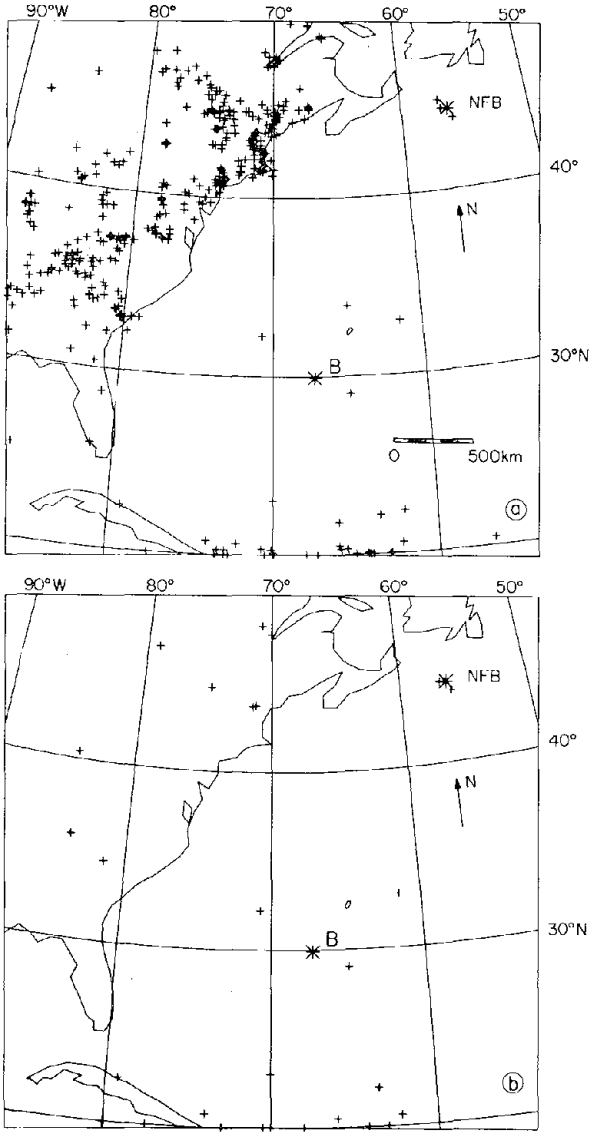

Fig. 10. (*a*) Map showing epicenters of all events in the time period 1900–1977 for eastern North America and the western Atlantic Ocean. Note that the two largest events in the offshore area are the Newfoundland Banks earthquake of November 18, 1929, $M = 7.2$ (NFB) [*Stewart*, 1979] and the Bermuda earthquake (B). Note the relatively low level of seismic activity in the offshore area compared with the activity in eastern North America. (*b*) Map showing epicenters of $M \geq 5.0$ events in the time period 1900–1977 for eastern North America and the western Atlantic Ocean. The seismicity in the offshore region is of comparable amount to the activity in eastern North America. Seismicity is taken from the USGS/NOAA worldwide catalogue in both Figures 10*a* and 10*b*.

Heezen and Fornari [1975] and *Schouten and Klitgord* [1980] the magnetic lineations are seen to trend in a northeast or north-northeast direction (Figure 9) and so are quite different in strike from the mechanism of the Bermuda earthquake, suggesting that the event is not associated with these. As seen in Figure 9, the epicenter lies just to the southeast of anomaly M11. From this figure, it can be seen that the now presumed inactive faults, which are the western extensions of the active transform fault system between the ridge crests of the Mid-Atlantic Ridge system, also change strike across this part of the western Atlantic. Between magnetic anomalies M18 and M11 the strike is west-northwest, while to the southeast of M11 the strike is more northwesterly. In the epicentral region of the Bermuda event, near the western extension of the Kane Fracture Zone, the strike of these features is approximately northwest (Figure 9), in reasonable agreement with the mechanism determined in this study.

The class of earthquakes which are referred to as intraplate events have received much attention recently due to the hazard they pose by way of damage and loss of life in areas which are poorly prepared for their occurrence. Perhaps the most dramatic example of the 1976 Tangshan, China, earthquake in which over 650,000 people lost their lives, illustrates this point well. It was estimated by *Butler et al.* [1978] to be one of the largest continental intraplate events to have occurred recently. Although China and Asia as a whole host many of the large continental intraplate events, other continental environments have not been devoid of such. In particular, within eastern North America, many events have occurred in the time period 1900–1977, as shown in Figure 10*a*. Several of these have been of magnitude $M \geq 5.0$ (Figure 10*b*). Two, in particular, were events of magnitude $M \geq 7$, viz. the 1925 La Malbaie, Canada, event (7.0) and the 1929 Newfoundland Banks earthquake (7.2) [*Stewart*, 1979]. Also, prior to 1900, several significant events occurred in eastern North America. Notable among them are the 1811–1812 New Madrid events in southeastern Missouri and the 1886 Charleston, South Carolina, earthquake. Intraplate activity, however, occurs not only within continental plates but within oceanic plates as well, the Hawaiian earthquake of November 29, 1975, being one of the largest examples. The focus of this study, the Bermuda earthquake, is another significant oceanic intraplate event.

The Bermuda earthquake is the largest seismically recorded

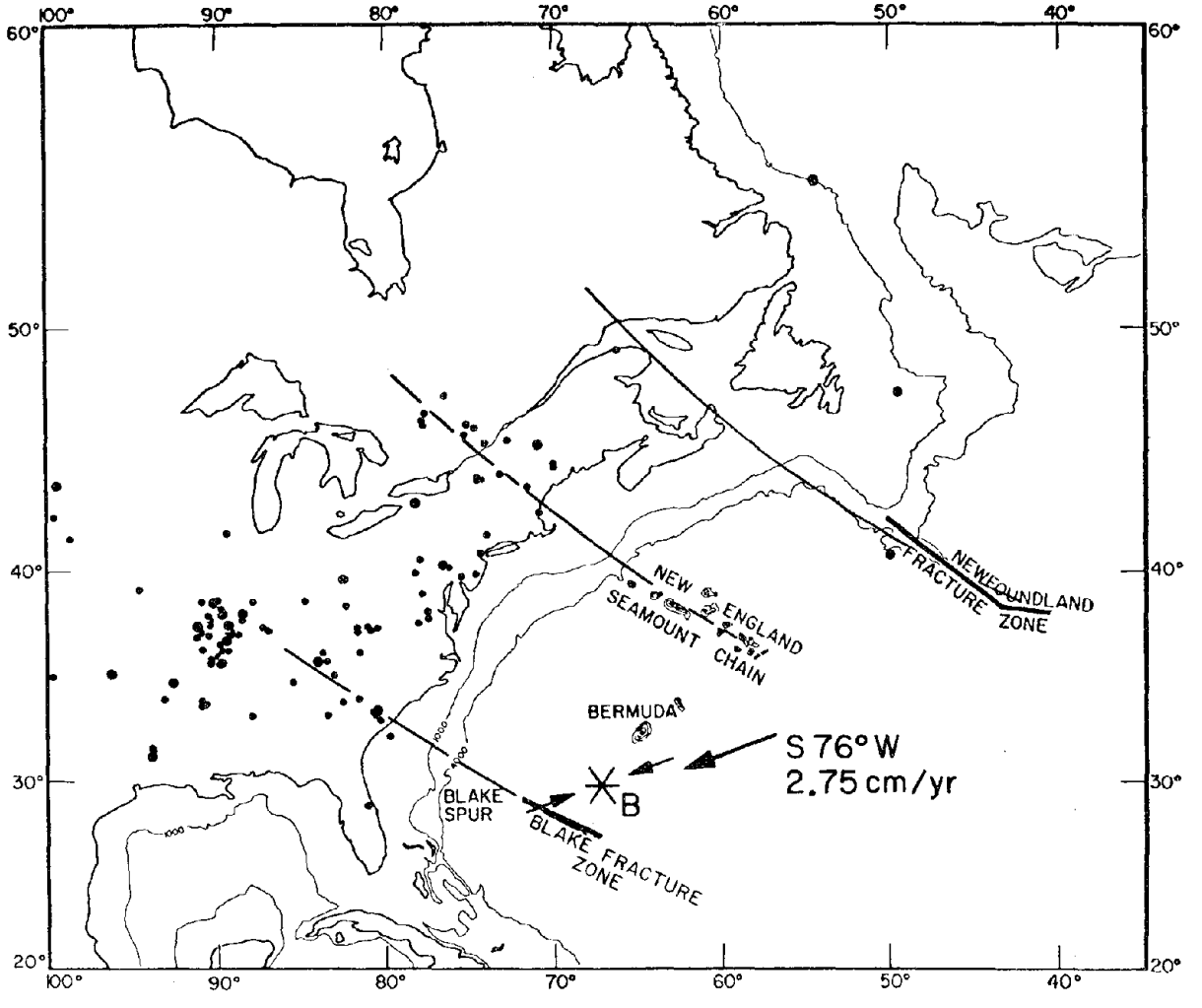

Fig. 11. The location of the Bermuda earthquake of March 24, 1978 (B), is shown along with the direction of maximum compression associated with it, determined in this study (small arrows). The large arrow indicates the direction of absolute plate motion of the North American plate at the epicenter of the Bermuda earthquake, calculated from *Minster and Jordan* [1978]. This figure is modified from *Sykes* [1978].

event to occur in the oceanic plate off the eastern coast of North America. As shown in Figures 10*a* and 10*b*, one other large event, the 1929 Newfoundland Banks earthquake (NFB) is located offshore in the region of the continental shelf [*Stewart*, 1979]. From studying Figure 10*a* one might consider the Bermuda event to be located in a region of relative seismic quiescence compared with the rest of eastern North America. However, since we have shown events of all magnitudes in the time period 1900–1977 in this plot, it is reasonable to assume that more events are located onshore due to the presence of a large number of seismographic stations in this region and hence better recording capability for smaller events compared with events offshore. To test this, we have plotted events of magnitude $M \geq 5.0$ for the same region. Magnitude of 5.0 probably represents the detection threshold for events in the offshore area. The result, shown in Figure 10*b*, indicates that the seismicity in the western Atlantic appears to be at a level similar to that in eastern North America.

The intraplate events discussed above appear to be present within all plates. Recently, *Sykes* [1978] reviewed intraplate seismicity and suggests that its origin may be related to the reactivation of preexisting zones of weakness. In particular, *Fletcher et al.* [1978] suggest that the Newfoundland Fracture Zone, the New England Seamount Chain, and the Blake Fracture Zone perhaps control the location of eastern North American seismicity (Figure 11). Assuming their hypothesis is correct and in the absence of any recent large seismic event, perhaps the Bermuda event can be considered as an analog for earthquake hazards prediction for the eastern seaboard. That is, the suggested style of faulting is relatively deep and of a thrusting nature. The consequence of these features on strong motion estimation is substantial.

Estimating earthquake hazards is a relatively difficult task because of the large number of unknowns involved. Fortunately, a substantial number of strong motion recordings have been obtained from recent events on the west coast which can be used to great advantage. For example, the San Fernando experience can be contrasted with what happened during the Santa Barbara event; both had thrust mechanisms with the latter being a deeper event. A relatively large amount of energy release occurred near the surface in the San Fernando situation, as reported on by *Heaton and Helmberger* [1979], and as a consequence, the microzonation techniques were not very successful [e.g., see *Hudson*, 1972]. Microzonation techniques assume that the seismic waves are traveling vertically near the surface, which is probably not the case in this situation. On the other hand, the strong motions produced by the Santa Barbara earthquake show a considerable degree of variability which can be explained by near-surface geology, as discussed by *Wallace and Helmberger* [1981]. Thus, microzonation methods can be expected to be far more effective in situations involving deep sources. There are many other effects involving attenuation, the relationship of intensity maps to mechanisms, etc., which are influenced by the style of faulting and are better discussed elsewhere. In short, a detailed analysis of the larger historic events in this region should be conducted to test the above assertion on the style of faulting.

CONCLUSIONS

As the largest event to occur recently, close to the eastern seaboard of North America, the Bermuda earthquake was worthy of study in an attempt to elucidate its tectonic origin. From studying a well-recorded body wave data set, the source mechanism for the Bermuda earthquake is constrained to be a north-northwest striking pure thrust mechanism (strike = N20°W, dip = 42°NE, rake = 90°) with the hypocenter located at a depth of 11 km, predominantly in the mantle. The event had a seismic moment of 3.4×10^{25} dyne cm determined from *P* wave data, while a value of 3.1×10^{25} dyne cm was determined from long-period Rayleigh wave data recorded by the IDA network. The north-northwest strike of the event is in good agreement with the bathymetry of the area, the epicenter being close to the southwestern edge of the Bermuda Rise. The strike of the Bermuda source mechanism (north-northwest) is close to the northwesterly strike of the presumed inactive fracture zones in the western Atlantic, suggesting that one of these zones acted as a nucleus for the event. The results from this study indicate that the direction of maximum compression for the Bermuda earthquake source is orientated in an east-northeast, west-southwest direction (small arrows in Figure 11). This direction is in remarkably good agreement with the direction of absolute motion of the North American plate (S76°W) at the epicenter of the Bermuda event calculated from *Minster and Jordan* [1978].

Acknowledgments. We would like to thank the personnel of all the WWSSN stations who were kind enough to send us seismograms. We thank Hans Schouten for useful discussions and allowing us to publish Figure 9. This research was supported by a grant from the National Academy of Sciences, through WDC-A seismology, the Division of Earth Sciences, National Science Foundation, NSF grant EAR78-14786, the Office of Naval Research contract 14-76-C-1070, and the Advanced Research Projects Agency of the Department of Defense and was monitored by the Air Force Office of Scientific Research under contract F49620-81-C-0008. Contribution 3337 Division of Geological and Planetary Sciences, California Institute of Technology, Pasadena, California.

REFERENCES

Agnew, D., J. Berger, R. Buland, W. Farrell, and F. Gilbert, International deployment of accelerometers: A network for very long-period seismology, *Eos Trans. AGU, 57*, 180–188, 1976.

Butler, R., G. S. Stewart, and H. Kanamori, The July 27, 1976 Tangshan, China earthquake—A complex sequence of intra-plate events, *Bull. Seismol. Soc. Am., 69*, 207–220, 1978.

Chase, T. E., Topography of the oceans, *IMR Tech. Rep. Ser. TR57*, Scripps Inst. of Oceanogr., La Jolla, Calif., 1975.

Douglas, A., J. B. Young, and J. A. Hudson, Complex *P*-wave seismograms from simple earthquake sources, *Geophy. J. R. Astron. Soc., 37*, 141–150, 1974.

Ewing, M., G. H. Sutton, and C. B. Officer, Jr., Seismic refraction measurements in the Atlantic Ocean, VI, Typical deep stations, North America basin, *Bull. Seismol. Soc. Am., 44*, 21–38, 1954.

Fletcher, J. B., M. L. Sbar, and L. R. Sykes, Seismic trends and traveltime residuals in eastern North America and their tectonic implications, *Geol. Soc. Am. Bull., 89*, 1656–1676, 1978.

Harkrider, D. G., Surface waves in multilayered elastic media, I, Rayleigh and Love waves from buried sources in a multilayered elastic half-space, *Bull. Seismol. Soc. Am., 54*, 627–679, 1964.

Heaton, T. H., and D. V. Helmberger, Generalized ray models of the San Fernando earthquake, *Bull. Seismol. Soc. Am., 69*, 1311–1342, 1979.

Heezen, B. C., and D. J. Fornari, Geological map of the Pacific Ocean, *Initial Rep. Deep Sea Drill. Proj., 30*, 1975.

Helmberger, D. V., and G. R. Engen, Upper mantle shear structure, *J. Geophys. Res., 79*, 4017–4028, 1974.

Hudson, D. E., Local distribution of strong earthquake ground motions, *Bull. Seismol. Soc. Am., 62*, 1765–1786, 1972.

Kanamori, H., and J. W. Given, Use of long-period surface waves for fast determination of earthquake source parameters, *Phys. Earth Planet. Inter.*, in press, 1981.

Kanamori, H., and G. S. Stewart, Seismological aspects of the Guatemala earthquake of February 4, 1976, *J. Geophys. Res., 83*, 3427–3434, 1978.

Langston, C. A., Body wave synthesis for shallow earthquake sources: Inversion for source and earth structure parameters, Ph.D. thesis, Calif. Inst. of Technol., Pasadena, 1976.

Langston, C. A., The February 9, 1971 San Fernando earthquake, *Bull. Seismol. Soc. Am., 68,* 1–30, 1978.

Langston, C. A., and R. Butler, Focal mechanism of the August 1, 1975 Oroville earthquake, *Bull. Seismol. Soc. Am., 66,* 1111–1120, 1976.

Langston, C. A., and D. V. Helmberger, A procedure for modeling shallow dislocation sources, *Geophys. J. R. Astron. Soc., 42,* 117–130, 1975.

Minster, J. B., and T. H. Jordan, Present-day plate motions, *J. Geophys. Res., 83,* 5331–5354, 1978.

Nishenko, S. P., H. Rowlett, G. M. Purdy, and J. Ewing, 1978 Bermuda earthquake—Main shock and aftershock studies, paper presented at Seismological Society of America, eastern section meeting, Weston, Mass., 1978.

Officer, C. B., M. Ewing, and P. C. Wuenschel, Seismic refraction measurements in the Atlantic Ocean, IV, Bermuda, Bermuda Rise and Nares Basin, *Geol. Soc. Am. Bull., 63,* 777–808, 1952.

Rial, J. A., The Caracas, Venezuela earthquake of July, 1967: A multiple source event, *J. Geophys. Res., 83,* 5405–5414, 1978.

Schouten, H., and K. D. Klitgord, Magnetic evidence for the persistence of minor offsets in the central north Atlantic mesozoic lineations, submitted to *J. Geophys. Res.*, 1980.

Shuran, E. M. (Ed.), World bathymetric map published by the chief administration for geodesy and cartography of the USSR, Moscow, 1971.

Stewart, G. S., The Grand Banks earthquake of November 18, 1929 and the Bermuda earthquake of March 24, 1978—A comparative study in relation to their intraplate location (abstract), *Eos Trans. AGU, 60,* 312, 1979.

Stewart, G. S., and D. V. Helmberger, Lateral variation in upper mantle structure suggested by waveform data from the Bermuda earthquake (abstract), *Eos Trans. AGU, 60,* 318, 1979.

Stewart, G. S., and H. Kanamori, Complexity of rupture propagation in large earthquakes (abstract), *Eos Trans. AGU, 59,* 1127, 1978.

Sykes, L. R., Intraplate seismicity, reactivation of preexisting zones of weakness, alkaline magmatism and other tectonism postdating continental fragmentation, *Rev. Geophys. Space Phys., 16,* 621–688, 1978.

Wallace, T. C., and D. V. Helmberger, An analysis of the strong-ground motion of the August 13, 1978 Santa Barbara earthquake, submitted to *Bull. Seismol. Soc. Am.*, 1981.

Ward, S., Ringing *P* waves and submarine faulting, *J. Geophys. Res., 84,* 3057–3062, 1979.

(Received July 29, 1980;
revised April 2, 1981;
accepted April 16, 1981.)